Two-photon transport in a waveguide coupled to a cavity in a two-level system

T. Shi (石弢),[1] Shanhui Fan (范汕洄),[2] and C. P. Sun (孙昌璞)[1]
[1]*Institute of Theoretical Physics, Chinese Academy of Sciences, Beijing 100190, China*
[2]*Ginzton Laboratory, Stanford University, Stanford, California 94305, USA*
(Received 20 September 2010; published 1 December 2011)

We study two-photon effects for a cavity quantum electrodynamics system where a waveguide is coupled to a cavity embedded in a two-level system. The wave function of two-photon scattering is exactly solved by using the Lehmann-Symanzik-Zimmermann reduction. Our results about quantum statistical properties of the outgoing photons explicitly exhibit the photon blockade effects in the strong-coupling regime. These results agree with the observations of recent experiments.

DOI: 10.1103/PhysRevA.84.063803 PACS number(s): 42.50.Pq, 42.79.Gn, 42.50.Ar, 11.55.Ds

I. INTRODUCTION

The Jaynes-Cummings (JC) system, involving cavity quantum electrodynamics (QED) for a two-level atom inside a cavity, is of most importance for quantum optics [1] and its applications. In the past decade, the JC system has been very extensively studied due to its potential applications for both quantum information processing and quantum device physics [2]. The latter is usually based on some solid-state systems, such as the superconducting circuit QED systems [3] and optomechanical architectures [4–6]. Recent experiments about various JC systems include demonstrations of on-chip cavities coupling to atoms or atomlike objects [7–12], and the integration of such atom-cavity systems with waveguides [13–15].

Recently, many experiments displayed a photon blockade phenomenon [16–18] in the JC system [19–21]. The photon blockade effect is an analogy of the "Coulomb blockade" effect. The strong Coulomb interaction between electrons results in the Coulomb blockade effect, however, according to QED, the direct interaction between photons vanishes. In order to generate a strong photon-photon interaction, in 1997 Imamoglu *et al.* proposed using the four-level nonlinear medium to realize the strong interaction between photons. In such systems, the excitation of the nonlinear medium by a first photon blocks the transport of a second photon, which is the photon blockade effect. As a result, after scattering by the nonlinear medium, the outgoing antibunched photons effectively repulse each other and show the sub-Poissonian statistics. Subsequently, a sequence of theoretical works [22–24] predicted the perfect antibunching behaviors in some nonlinear systems. In the experimental works, some profound results have been explored, for example, the photon blockade effect has been observed in a single-exciton recombination enclosed in a photonic cavity [25]. Furthermore, the strong-coupling regime of the JC system was achieved in the microcavity with a single quantum dot [26,27], thus, one studied the photon blockade in the JC system [19–21] in the strong-coupling regime. Recently, photon blockade effects have also been extensively studied in circuit QED systems [28], optical nanocavity systems [29], strong correlated systems [30], and cold atom systems [31].

In this paper, we focus on the photon blockade effects observed in the experiment [19]. The authors utilized the JC system as the nonlinear medium to generate the strong-coupling effect of photons. They found that when the driven light resonated with the single-photon dressed states of the JC system, the outgoing photons exhibit the manifested antibunching behaviors. The experiments have thus demonstrated nonlinearity at a single-photon level, which is crucial for generating [16] and detecting single photons. For comprehensive understanding of the photon blockade effect of the JC system, we need to study the intensity and coherence properties of transmitted or reflected light, when a few photons are injected into the system through a waveguide. In Refs. [19,32], the quantum states inside the cavity were expanded on a basis of photon number states. Truncating the number of basis states then reduced the master equations to an ordinary differential equation which can be solved numerically. This system has also been simulated by using the quantum trajectory approach [33]. Analytically, closed-form formulas regarding the transmission and coherence properties have been obtained, either in the weak excitation limit where the atom is assumed to be mostly in the ground state [34,35], or in a mean-field-like approach where the expectation value of the operator product is taken as the product of operator expectation values [36]. Given that the JC systems will be ultimately used for quantum information processing and quantum optics, understanding their response to few-photon states other than coherent states is very important, especially for understanding the photon blockade effect regarding a single-photon source and the detecting apparatus at a single-photon level.

Here, in contrast to most existing theoretical works that used coherent-state input, we focus on the two-photon and few-photon input. The two-photon transports can be considered as a scattering process. To study the statistics of the outgoing photons, we need the scattering matrix which transforms the in state to the out state. Fortunately, the scattering matrix relates the Green function of photons by the Lehmann-Symanzik-Zimmermann (LSZ) [37] reduction in quantum field theory, and the Green function can be obtained exactly for the linear waveguide photons. The field-theoretic techniques [38], without any approximation, provide an exact analytic formula for the two-photon scattering in the system shown in Fig. 1. Our results for two photons show that in the strong-coupling case the outgoing photons exhibit strong antibunching behaviors, which can explain the photon blockade phenomenon observed in the experiment [19]. We emphasize that the antibunching behaviors and sub-Poissonian

 ©2011 American Physical Society

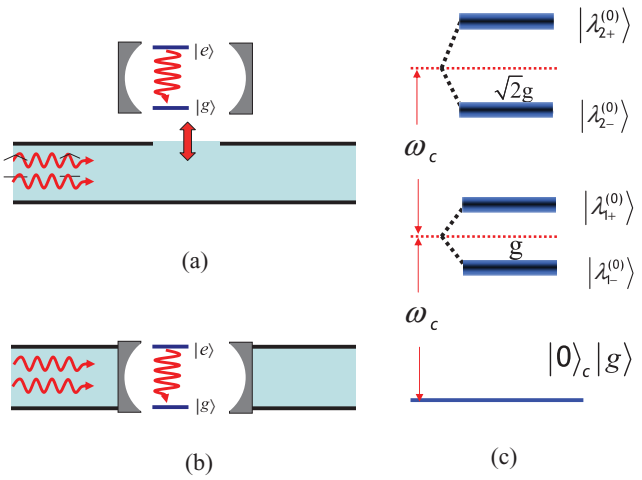

FIG. 1. (Color online) Two kinds of coupling structures and the schematic of the energy spectrum. (a) The side-coupled waveguide. (b) The direct-coupled waveguide. (c) The schematic for the energy spectrum of the JC model in the subspaces $n = 0$, 1, and 2.

statistics result from the incommensurate energy spectrum of the JC systems.

II. TRANSPORT MODEL AND *S* MATRIX

Two configurations [39,40], where the atom-cavity system is either side coupled [41–44] or directly coupled [19,32] to a waveguide, are schematically shown in Figs. 1(a) and 1(b), respectively. In this paper, we focus on the side-coupling case. The system in Fig. 1(a) is described by a Hamiltonian $H = H_{\rm W} + H_{\rm JC} + H_{\rm I}$ containing three parts: (a) the waveguide Hamiltonian

$$H_{\rm W} = \sum_k \varepsilon_k a_k^\dagger a_k, \tag{1}$$

where a_k ($a_k^\dagger$) denotes the annihilation (creation) operators of the photon; $\varepsilon_k = v|k|$ is the waveguide dispersion relation, and we take the speed of light v as unity; (b) the JC Hamiltonian for the coupling of the cavity field to the two-level system (TLS)

$$H_{\rm JC} = \omega_c a^\dagger a + \Omega|e\rangle\langle e| + g(a^\dagger|g\rangle\langle e| + a|e\rangle\langle g|), \tag{2}$$

where a ($a^\dagger$) denotes the annihilation (creation) operators of the photon in the cavity with frequency ω_c, $|e\rangle$ ($|g\rangle$) denotes the excited (ground) state of the TLS with energy-level spacing Ω, and g is the coupling constant of the TLS and the cavity field; and (c) the term

$$H_{\rm I} = \frac{V}{\sqrt{L}} \sum_k (a_k^\dagger a + {\rm H.c.}) \tag{3}$$

describing the coupling between the cavity and the waveguide. Here, V is the waveguide-cavity coupling constant and L is the length of the waveguide. In the following, for convenience, we use the fermion representation of the TLS, i.e., $|e\rangle\langle e| = f_e^\dagger f_e$ and $|g\rangle\langle e| = f_g^\dagger f_e$, by two fermion annihilation (creation) operators f_e and f_g ($f_e^\dagger$ and $f_g^\dagger$), respectively. Notice that for the TLS, the constraint $f_e^\dagger f_e + f_g^\dagger f_g = 1$ is required.

With respect to the bonding and antibonding waveguide modes defined by

$$\begin{aligned} e_k &= \frac{1}{\sqrt{2}}(a_k + a_{-k}), \\ o_k &= \frac{1}{\sqrt{2}}(a_k - a_{-k}), \end{aligned} \tag{4}$$

H is decomposed into two parts:

$$H_{\rm e} = \sum_{k>0} k e_k^\dagger e_k + \frac{\tilde{V}}{\sqrt{L}} \sum_{k>0} (e_k^\dagger a + {\rm H.c.}) + H_{\rm JC}, \tag{5}$$

and $H_{\rm o} = \sum_{k>0} k o_k^\dagger o_k$, where $\tilde{V} = \sqrt{2}V$. For the antibonding part, the LSZ reduction [38] is used to calculate the S-matrix elements with input and output photon momenta $\mathbf{k} = k_1,\ldots,k_n$ and $\mathbf{p} = p_1,\ldots,p_n$.

Using the diagrammatic analysis, we find that the Feynman diagram of S-matrix elements for two incident photons with momenta, i.e., k_1 and k_2, and two outgoing photons with momenta, i.e., p_1 and p_2, can be reduced to three kinds of disconnected diagrams, (a), (b), and (c) as shown in Fig. 2. By summing up the contributions from these disconnected diagrams, we obtain the two-photon S-matrix element

$$S_{p_1 p_2 k_1 k_2} = S_{p_1 k_1} S_{p_2 k_2} + S_{p_2 k_1} S_{p_1 k_2} + i T_{p_1 p_2 k_1 k_2}, \tag{6}$$

which is determined by the single-photon S-matrix element $S_{pk} = \delta_{pk} + iT_{pk}$ and the two-photon T-matrix element $T_{p_1 p_2 k_1 k_2}$, where T_{pk} is the single-photon T-matrix element.

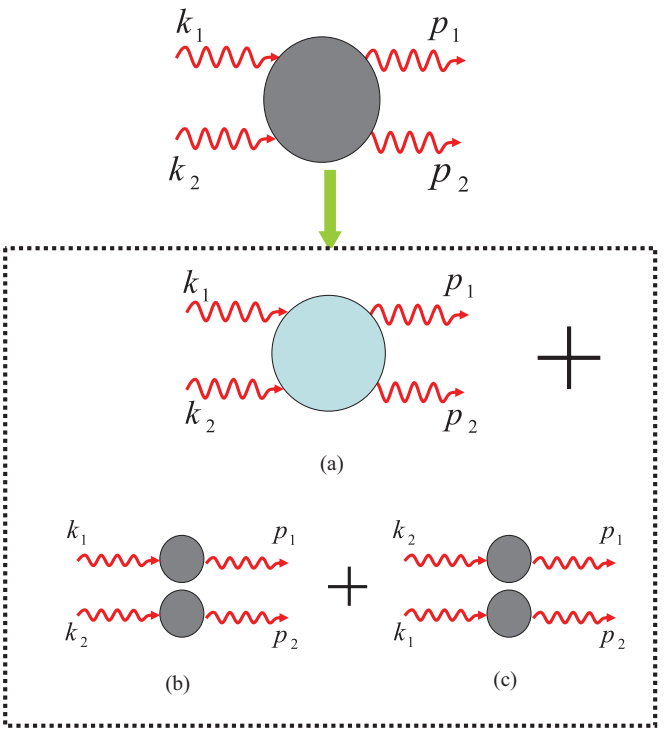

FIG. 2. (Color online) The diagrammatic constructions of the two-photon S-matrix element: There exist three kinds of disconnected diagrams, (a), (b), and (c). The red wavy line denotes the free photon propagator. The gray dark circles denote the S-matrix elements and the blue bright circle denotes the two-photon T-matrix elements.

Generally, the intrinsic relation

$$T_{[\mathbf{p};\mathbf{k}]} = \frac{i(2\pi)^n G_{[\mathbf{p};\mathbf{k}]}(\omega_{\mathbf{p}},\omega_{\mathbf{k}})}{\prod_{j=1}^{n}[G_0(\omega_{p_j},p_j)G_0(\omega_{k_j},k_j)]}, \tag{7}$$

between the T-matrix element $T_{[\mathbf{p};\mathbf{k}]}$ and the connected Green function

$$G_{[\mathbf{p};\mathbf{k}]}(\omega_{\mathbf{p}},\omega_{\mathbf{k}}) = \int \prod_{j=1}^{n}\left[\frac{dt_j\,dt_j'}{2\pi}\right] G_{[\mathbf{p};\mathbf{k}]}(\mathbf{t}',\mathbf{t}) \times \prod_{j=1}^{n}[-\exp(i\omega_{p_j}t_j' - i\omega_{k_j}t_j)] \tag{8}$$

is given by the LSZ reduction approach, where $\omega_{p_j} = p_j$, $\omega_{k_j} = k_j$, and

$$G_0(\omega_p,p) = \frac{i}{\omega_p - \varepsilon_p + i0^+} \tag{9}$$

is the bare Green function. Since we focus on the two photons scattering in vacuum, the zero-temperature Green function $G_{[\mathbf{p};\mathbf{k}]}(\mathbf{t}',\mathbf{t})$,

$$G_{[\mathbf{p};\mathbf{k}]}(\mathbf{t}',\mathbf{t}) = \left.\frac{\delta^{2n}\ \ln\ Z[\eta_k,\eta_k^*]}{\delta\eta_{p_1}^*(t_1')\cdots\delta\eta_{p_n}^*(t_n')\delta\eta_{k_1}(t_1)\cdots\delta\eta_{k_n}(t_n)}\right|_{\substack{\eta_k=0\\ \eta_k^*=0}}, \tag{10}$$

is considered for $\mathbf{t} = t_1,\ldots,t_n$ and $\mathbf{t}' = t_1',\ldots,t_n'$, where in order to obtain $G_{[\mathbf{p};\mathbf{k}]}(\mathbf{t}',\mathbf{t})$, we use the functional integral approach [38], which is widely applied in quantum optics [45,46], to write the generating functional

$$Z[\eta_k,\eta_k^*] = \int D[e_k]D[e_k^*]D[a]D[a^*]D[\sigma] \times \exp\left\{i\int dt\left[L_{\mathrm{e}} + \sum_{k>0}(\eta_k^* e_k + \mathrm{H.c.})\right]\right\}, \tag{11}$$

which is the vacuum-vacuum transition amplitude. The functional measure

$$D[\sigma] = D[f_e]D[f_e^*]D[f_g]D[f_g^*]\delta(f_e^* f_e + f_g^* f_g - 1) \tag{12}$$

for the variables of the TLS is a bit complex, because we need to consider the constraint $f_e^\dagger f_e + f_g^\dagger f_g = 1$ in the fermion representation of TLS. Here, we have used the c numbers (e_k and a) and the Grassmann numbers (f_e and f_g), and the Lagrangian is

$$L_{\mathrm{e}} = i\sum_k e_k^*\partial_t e_k + ia^*\partial_t a + i\sum_{\sigma=e,g} f_\sigma^*\partial_t f_\sigma - H_{\mathrm{e}}. \tag{13}$$

By integrating out the photon field e_k, we obtain

$$\ln\ Z[\eta_k,\eta_k^*] = \ln\ Z_{\mathrm{eff}}[\xi,\xi^*] - i\int d\omega\sum_k \frac{|\eta_k(\omega)|^2}{\omega - \varepsilon_k + i0^+}, \tag{14}$$

with the effective functional

$$Z_{\mathrm{eff}}[\xi,\xi^*] = \int D[a]D[a^*]D[\sigma] \times \exp\left\{i\int dt\ L_{\mathrm{eff}} + i\int dt(\xi^* a + \xi a^*)\right\}, \tag{15}$$

where we define the effective Lagrangian

$$L_{\mathrm{eff}} = ia^*\partial_t a + i\sum_{\sigma=e,g} f_\sigma^*\partial_t f_\sigma - H_{\mathrm{eff}}, \tag{16}$$

and the effective non-Hermite Hamiltonian

$$H_{\mathrm{eff}} = \alpha a^* a + \Omega f_e^* f_e + g(a^* f_g^* f_e + \mathrm{H.c.}). \tag{17}$$

We introduce $\alpha = \omega_c - i\tilde{V}^2/2$, and a new external source $\xi(t) = \int d\omega\,\xi(\omega)e^{-i\omega t}/\sqrt{2\pi}$ by

$$\xi(\omega) = \frac{\tilde{V}}{\sqrt{L}}\sum_k \frac{\eta_k(\omega)}{\omega - \varepsilon_k + i0^+}. \tag{18}$$

A. Single-photon scattering

For the single-photon case, Eq. (7) leads to

$$iT_{pk} = 2\pi G_{pk}(\omega_p,\omega_k)G_0^{-1}(\omega_p,p)G_0^{-1}(\omega_k,k)|_{\omega_p=\varepsilon_p,\omega_k=\varepsilon_k} \tag{19}$$

by cutting the external legs $G_0(\omega_p,p)$ and $G_0(\omega_k,k)$ for the exact Green's function $G_{pk}(\omega_p,\omega_k)$, where $iG_0^{-1}(\omega_p,p) = \omega_p - \varepsilon_p + i0^+$ is the free propagator of photon and

$$G_{pk}(\omega_p,\omega_k) = \int \frac{dt\,dt'}{2\pi}G_{pk}(t',t)e^{i\omega_p t' - i\omega_k t}. \tag{20}$$

From Eq. (10), we obtain the two-point time-ordering connected Green's function

$$G_{pk}(t',t) = -\left.\frac{\delta^2\ \ln\ Z[\eta,\eta^*]}{\delta\eta_p^*(t')\delta\eta_k(t)}\right|_{\eta=\eta^*=0}. \tag{21}$$

Together with Eqs. (14)–(18), Eq. (21) leads to

$$G_{pk}(\omega_p,\omega_k) = G_0(\omega_k,k)\delta_{pk}\delta(\omega_k - \omega_p) - \frac{\tilde{V}^2}{2\pi}G_0(\omega_p,p)G_0(\omega_k,k)G_c(\omega_p,\omega_k), \tag{22}$$

where we defined

$$G_c(\omega_p,\omega_k) = \int \frac{dt'\,dt}{2\pi}e^{i\omega_p t' - i\omega_k t}G_c(t',t), \tag{23}$$

by the correlation function of photon in the cavity as

$$G_c(t',t) = -\left.\frac{\delta^2\ \ln\ Z_{\mathrm{eff}}[\xi,\xi^*]}{\delta\xi^*(t')\delta\xi(t)}\right|_{\xi=\xi^*=0} = \langle Ta(t')a^\dagger(t)\rangle. \tag{24}$$

Here, $a(t) = e^{iH_{\mathrm{eff}}t}ae^{-iH_{\mathrm{eff}}t}$ and $a^\dagger(t) = e^{iH_{\mathrm{eff}}t}a^\dagger e^{-iH_{\mathrm{eff}}t}$. Finally, Eq. (19) leads to

$$iT_{pk} = -\tilde{V}^2\int \frac{dt'\,dt}{2\pi}e^{ipt' - ikt}\langle \mathcal{T}a(t')a^\dagger(t)\rangle, \tag{25}$$

where $\langle\mathcal{T}\ldots\rangle$ is the time-ordered average on the state $|0\rangle_{\mathrm{c}}|g\rangle$ with $|0\rangle_{\mathrm{c}}$ being the vacuum state of the cavity field.

B. Two-photon scattering

For the two-photon case, the T-matrix element is

$$iT_{p_1p_2k_1k_2} = G_{\{p_i\};\{k_i\}}(\{\omega_{p_i}\},\{\omega_{k_i}\}) \times \prod_{i=1,2}[2\pi G_0^{-1}(\omega_{p_i},p_i)G_0^{-1}(\omega_{k_i},k_i)]\Big|_{\substack{\omega_{p_i}=\varepsilon_{p_i},\\ \omega_{k_i}=\varepsilon_{k_i}}}. \quad (26)$$

Here, we denote $\{\omega_{p_i}\} = \{\omega_{p_1},\omega_{p_2}\}$, $\{p_i\} = \{p_1,p_2\}$, and

$$G_{\{p_i\};\{k_i\}}(\{\omega_{p_i}\},\{\omega_{k_i}\}) = \int \frac{dt_1'\,dt_2'\,dt_1\,dt_2}{(2\pi)^2} e^{i\omega_{p_1}t_1'+i\omega_{p_2}t_2'-i\omega_{k_1}t_1-i\omega_{k_2}t_2} \times G_{\{p_i\};\{k_i\}}(t_1',t_2',t_1,t_2). \quad (27)$$

The four-point time-ordering connected Green's function is

$$G_{\{p_i\};\{k_i\}}(t_1',t_2',t_1,t_2) = \frac{\delta^4 \ln Z[\eta,\eta^*]}{\delta\eta^*_{p_1}(t_1')\delta\eta^*_{p_2}(t_2')\delta\eta_{k_1}(t_1)\delta\eta_{k_2}(t_2)}\Big|_{\eta=\eta^*=0}, \quad (28)$$

and Eqs. (14)–(18) lead to

$$G_{\{p_i\};\{k_i\}}(\{\omega_{p_i}\},\{\omega_{k_i}\}) = \frac{\tilde{V}^4}{(2\pi)^2}G_c(\{\omega_{p_i}\},\{\omega_{k_i}\}) \times \prod_{i=1,2}[G_0(\omega_{p_i},p_i)G_0(\omega_{k_i},k_i)], \quad (29)$$

where we define

$$G_c(\{\omega_{p_i}\},\{\omega_{k_i}\}) = \int \frac{dt_1'\,dt_2'\,dt_1\,dt_2}{(2\pi)^2} G_c(\{t_i'\},\{t_i\}) \times e^{i\omega_{p_1}t_1'+i\omega_{p_2}t_2'-i\omega_{k_1}t_1-i\omega_{k_2}t_2} \quad (30)$$

by the connected correlation function of photons in the cavity as

$$G_c(\{t_i'\},\{t_i\}) = \frac{\delta^4 \ln Z_{\rm eff}[\eta_k,\eta_k^*]}{\delta\xi^*(t_1')\delta\xi^*(t_2')\delta\xi(t_1)\delta\xi(t_2)}\Big|_{\eta_k=\eta_k^*=0} = \langle \mathcal{T}a(t_1')a(t_2')a^\dagger(t_1)a^\dagger(t_2)\rangle \equiv G_4. \quad (31)$$

Finally, Eq. (26) leads to

$$iT_{p_1p_2k_1k_2} = \frac{\tilde{V}^4}{2\pi}\int\left(\prod_{j=1,2} dt_j\,dt_j'\,e^{ip_jt_j'-ik_jt_j}\right)G_4. \quad (32)$$

C. Exact T-matrix elements

In an invariant subspace with the eigenvalue n of the excitation number operator

$$N = |e\rangle\langle e| + a^\dagger a, \quad (33)$$

$H_{\rm eff}$ is diagonalized with the eigenstates

$$|\lambda_{n\pm}\rangle = \mathcal{N}_{n\pm}\{-\sqrt{n}g|n-1\rangle_{\rm e}|e\rangle + [\Omega+(n-1)\alpha-\lambda_{n\pm}]|n\rangle_{\rm e}|g\rangle\}, \quad (34)$$

and the corresponding eigenvalues

$$\lambda_{n\pm} = \tfrac{1}{2}\{\Omega+(2n-1)\alpha \pm [(\Omega-\alpha)^2+4ng^2]^{1/2}\}, \quad (35)$$

where $\mathcal{N}_{n\pm}$ are the normalization constants. The schematic for the spectrum of the JC model is shown in Fig. 1(c). We notice that the eigenstates $|\lambda_{n\pm}\rangle$ are not orthogonal to each other. Thus, in the following calculations, we need to use the biorthogonal basis approach [47] with the eigenstates

$$|\lambda^*_{n\pm}\rangle = \mathcal{N}_{n\pm}\{-\sqrt{n}g|n-1\rangle_{\rm e}|e\rangle + [\Omega+(n-1)\alpha^*-\lambda^*_{n\pm}]|n\rangle_{\rm e}|g\rangle\}, \quad (36)$$

of $H^*_{\rm eff} = H_{\rm eff}|_{\alpha\to\alpha^*=\omega_c+i\tilde{V}^2/2}$ corresponding to the eigenvalues $\lambda^*_{n\pm}$. The orthogonal relations are $\langle\lambda^*_{n\mp}|\lambda_{n\pm}\rangle = 0$ and $\langle\lambda^*_{n\pm}|\lambda_{n\pm}\rangle = 1$.

In the above biorthogonal basis, we can evaluate the correlations $\langle\mathcal{T}a(t')a^\dagger(t)\rangle$ and G_4, to obtain the single-photon and two-photon T matrices and S matrices. The results are listed as follows: (1) For the bonding modes, the single-photon S matrix is $S_{pk} = t_k\delta_{kp}$, where $t_k = \exp(-i2\delta_k)$ and phase shift $\delta_k = \arg[(k-\lambda_{1+})(k-\lambda_{1-})]$. The antibonding modes are free of coupling, and thus possess the S-matrix element $S^{(o)}_{pk} = \delta_{kp}$. (2) Then the single-photon reflection and transmission coefficients are obtained as $\bar{r}_k = (t_k-1)/2$ and $\bar{t}_k = (t_k+1)/2$, which agree with Ref. [39]. (3) The two-photon T-matrix elements are determined by Eq. (32), and obviously the Fourier transformation of G_4. The time-ordered Green function G_4 can be calculated straightforwardly in the Schrödinger representation, since the energy spectrum and the eigenstates of $H_{\rm eff}$ are both obtained. A sophisticated calculation leads to

$$iT_{p_1p_2k_1k_2} = \frac{i\tilde{V}^4g^4(E-\alpha-\Omega)\delta_{p_1+p_2,E}}{\pi\prod_{s=\pm}(E-\lambda_{2s})} \times \frac{[(E-2\Omega)(E-2\alpha)-4g^2]}{\prod_{s=\pm}\prod_{i=1,2}(k_i-\lambda_{1s})(p_i-\lambda_{1s})}, \quad (37)$$

where $E = k_1+k_2$ is the total energy of the incident photons. The system thus exhibits two-photon background fluorescence $T_2 = |T_{p_1p_2k_1k_2}|^2$ in the bonding mode.

III. TWO-PHOTON WAVE FUNCTIONS AND PHOTON STATISTICS

Let $a_R(x_1)$ $[a_L(x_2)]$ denote the annihilation operators of right- (left-) moving photons [48]. It follows from Eqs. (6) and (37) that the outgoing state $|X_{\rm out}\rangle = |t_{\rm out}\rangle + |r_{\rm out}\rangle + |rt_{\rm out}\rangle$ for two incident right-moving photons with momenta k_1 and k_2 contains three parts: (a) the quantum state of the two transmitted photons,

$$|t_{\rm out}\rangle = \int dx_1\,dx_2\,t_2(x_1,x_2)a_R^\dagger(x_1)a_R^\dagger(x_2)|0\rangle|g\rangle, \quad (38)$$

explicitly defined by the two-photon wave function

$$t_2(x_1,x_2) = \frac{1}{2\pi}e^{iEx_c}[\bar{t}_{k_1}\bar{t}_{k_2}\cos(\Delta_k x) - F(\lambda,x)], \quad (39)$$

where $\Delta_k = k_1 - k_2$ and

$$F(\lambda,x) = \frac{\tilde{V}^4 g^4 \sum_{s=\pm} s(E-2\lambda_{1s}) \exp[i(\frac{E}{2}-\lambda_{1,-s})|x|]}{4(\lambda_{1+}-\lambda_{1-})\prod_{s=\pm}[(E-\lambda_{2s})\prod_{i=1,2}(k_i-\lambda_{1s})]}, \tag{40}$$

and $x = x_1 - x_2$ and $x_c = (x_1 + x_2)/2$ are the relative and center-of-mass coordinates, respectively; (b) the quantum state of the two reflected photons,

$$|r_{\rm out}\rangle = \int dx_1\, dx_2\, r_2(x_1,x_2) a_L^\dagger(x_1) a_L^\dagger(x_2)|0\rangle|g\rangle, \tag{41}$$

explicitly defined by

$$r_2(x_1,x_2) = \frac{1}{2\pi} e^{-iEx_c}[\bar{r}_{k_1}\bar{r}_{k_2}\cos(\Delta_k x) - F(\lambda,x)]; \tag{42}$$

and (c) the left-right entangled two-photon state

$$|rt_{\rm out}\rangle = \int dx_1\, dx_2\, rt_2(x_1,x_2) a_L^\dagger(x_1) a_R^\dagger(x_2)|0\rangle|g\rangle \tag{43}$$

describing the scenario where one photon is transmitted while the other is reflected. Here,

$$rt_2 = \frac{1}{2\pi} e^{i(E/2)x}[(\bar{t}_{k_1}\bar{r}_{k_2}e^{2i\Delta_k x_c} + \bar{t}_{k_2}\bar{r}_{k_1}e^{-2i\Delta_k x_c}) - 2F(\lambda,2x_c)]. \tag{44}$$

Photon statistics can be studied through the coherence functions [1] $g^{(2)}(\tau) = G^{(2)}(\tau)/|G^{(1)}(0)|^2$, where

$$G^{(1)}(\tau) = \langle F_{\rm out}|a_F^\dagger(x+\tau)a_F(x)|F_{\rm out}\rangle,$$
$$G^{(2)}(\tau) = \langle F_{\rm out}|a_F^\dagger(x)a_F^\dagger(x+\tau)a_F(x+\tau)a_F(x)|F_{\rm out}\rangle, \tag{45}$$

and $F = R$ and L correspond to the transmitted photons and reflected photons, respectively, with $|R_{\rm out}\rangle = |t_{\rm out}\rangle/\langle t_{\rm out}|t_{\rm out}\rangle$ and $|L_{\rm out}\rangle = |r_{\rm out}\rangle/\langle r_{\rm out}|r_{\rm out}\rangle$. We have $g^{(2)}(\tau) = C(\tau)/D$, where $C(\tau) = |t_2(x,x+\tau)|^2$ for photons in transmission, and $|r_2(x,x+\tau)|^2$ for photons in reflection, which is independent of x and D is the normalization constant.

A. Strong-coupling regime

To explore the physical consequence of the result above, we first consider the strong-coupling regime with $\tilde{V}^2 < g < \Omega$. The two-photon background fluorescence T_2 and the correlation function $g^{(2)}(\tau)$ are shown in Fig. 3. We assume that the atom and cavity are on resonance, i.e., $\omega_c = \Omega$, and the same energy for the two incident photons, i.e., $\Delta_k = 0$. When the average energy of two photons $E/2 = \lambda_{1\pm}^{(0)}$, T_2 has one sharp peak at $\Delta_k = \Delta_p = 0$, and the four peaks emerge [see Fig. 3(a)] for $E = \lambda_{2\pm}^{(0)}$.

In Fig. 3(b), the single-photon reflection probability $|\bar{r}_{E/2}|^2$ and $g^{(2)}(0)$ as the functions of energy $E/2$ per photon are shown for the two reflected photons, respectively. The two reflected photons exhibit sub-Poissonian statistics [$g^{(2)}(0) \ll 1$] for $E/2 = \lambda_{1\pm}^{(0)}$, and super-Poissonian statistics [$g^{(2)}(0) \gg 1$] for $E/2 = \lambda_{2\pm}^{(0)}/2$ or Ω. For $E/2 = \lambda_{1\pm}^{(0)}$, the correlation functions $g^{(2)}(\tau)$ of two reflected [solid (blue) curve in Fig. 3(c)] and transmitted [dashed (red) curve in Fig. 3(d)] photons exhibit antibunching and bunching behaviors, respectively.

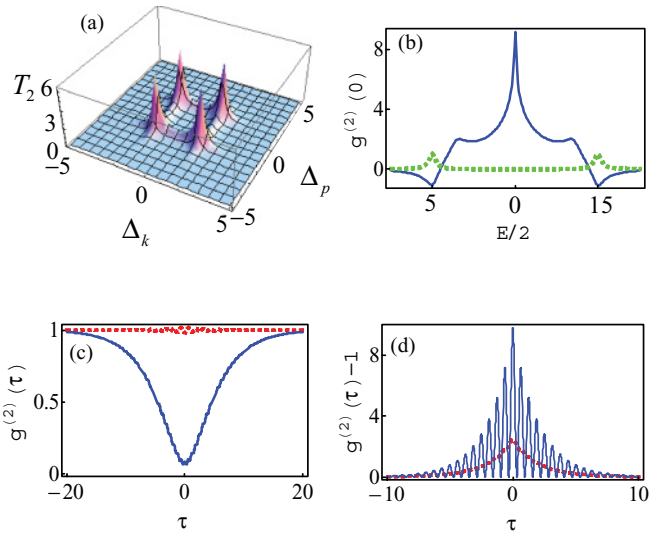

FIG. 3. (Color online) The two-photon background fluorescence and the correlation functions for the strong-coupling regime $g = 5$, where the system parameters are $\omega_c = \Omega = 10$ and $\tilde{V}$ is taken as unit: (a) two-photon background fluorescence for $E = \lambda_{2s}^{(0)}$; (b) $g^{(2)}(0)$ of the reflected [solid (blue) curve] photons, and the single-photon reflection probability $|\bar{r}_{E/2}|^2$ [dashed (green) curve]; (c) $g^{(2)}(\tau)$ of the reflected [solid (blue) curve] photons for $E/2 = \lambda_{1s}^{(0)}$ and transmitted [dashed (red) curve] photons for $E/2 = \Omega$; (d) $[g^{(2)}(\tau) - 1]/10^{15}$ of the reflected [solid (blue) curve] photons for $E/2 = \Omega$ and $[g^{(2)}(\tau) - 1]/10^6$ of transmitted [dashed (red) curve] photons for $E/2 = \lambda_{1s}^{(0)}$.

When $E/2 = \Omega$, $g^{(2)}(\tau)$ of two reflected [solid (blue) curve in Fig. 3(d)] and transmitted [dashed (red) curve in Fig. 3(c)] photons exhibit large bunching and antibunching behaviors, respectively.

In Ref. [19], the authors used the directly coupled cavity [Fig. 1(b)] to study the photon blockade effects. And in Fig. 2(a) of Ref. [19], they show that when the incident photons resonate with the single-photon dressed states $\lambda_{1\pm}^{(0)}$, the photon transmission coefficient reaches the maximum and the transmitted antibunched photons exhibit sub-Poissonian statistics. On the other hand, when each incident photon has the frequency $\lambda_{2\pm}^{(0)}/2$ or Ω, the transmitted bunched photons exhibit super-Poissonian statistics. Comparing Fig. 2(a) in Ref. [19] with Fig. 3(b) in our paper, we find that our results for the two reflected photons in the case of a side-coupled cavity exactly agree with that for the transmitted photons observed in the experiment [19] that used a directly coupled cavity. This agreement is not accidental, since there is a dual theorem [39] about these two configurations: the transmitted photon states in the direct-coupled case can be mapped into the reflected photon states in the side-coupled case. Using a transformation [39], we can prove the dual theorem by relating the right-moving and left-moving modes in the side-coupling waveguide [Fig. 1(a)] to the photon modes in the left waveguide and the right waveguide for the direct-coupling waveguide [Fig. 1(b)]. This transformation is also used in the low-dimensional condensed-matter system [49].

In the side-coupled structure considered here, the reflected light arises purely from the dressed TLS. Thus, single-photon

reflection peaks at the energy levels $\lambda_{1\pm}^{(0)}$ of one-photon dressed states in the cavity. Similarly, $g^{(2)}(0)$ for two-photon reflection peaks when the two-photon energy is $\lambda_{2\pm}^{(0)}$, where the cavity supports two-photon dressed states. However, since $\lambda_{2\pm}^{(0)} \neq 2\lambda_{1\pm}^{(0)}$, two photons each with energy $E/2 = \lambda_{1\pm}^{(0)}$ is off resonance from the two-photon dressed states. In such a case, the reflection of each photon reaches the maximum $|\bar{r}_{E/2}|^2 = 1$, and the single excitation by the first photon in fact prevents the second photon from entering the cavity, resulting in the photon-blockade effect and the generation of the antibunching photons (single photons) in reflection. Therefore, in contrast to the case of direct coupling where the photon-blockade effect manifests as a vanishing two-photon transmission, in the side-cavity case the photon blockade effect manifests as a vanishing two-photon reflection effect. When $E/2 = \Omega$, the single-photon reflection coefficient vanishes [39]. The two-photon reflection is due purely to the correlation induced by the TLS, which creates a two-photon bound state, and hence generates a large bunching effect [32]. The strong antibunching in reflection implies that this system in the strong-coupling regime might be used as a single-photon source. Our analysis shows that the photon-blockade effect and the generation of antibunching photons originate from the incommensurate energy spectra [Fig. 1(c)] of the cavity and the TLS. Here, the incommensurate energy spectra means that the energy level of the system cannot be expressed as $E_n = n\omega_0$ with the integer n. Thus, when the first photon of the incident energy ε_R on resonance with the single excitation of the system is absorbed, the system would not like to absorb the second photon with the same incident energy ε_R, since the $2\varepsilon_R$ is not resonant with any energy level of the system due to the incommensurate energy spectrum. We, therefore, provide an exact analytic formula for the photon correlation function, the special case of which completely agrees with the existing experimental data.

B. Weak-coupling regime

We now examine the weak-coupling regime with $g < \tilde{V}^2$. As shown in Fig. 4, unlike the strong-coupling case [Fig. 3(a)], here the background fluorescence exhibits a single peak when $E = \lambda_{2\pm}^{(0)}$.

We find that $g^{(2)}(0)$ of the two reflected photons [Fig. 4(b)] has a simple structure with one peak at $E/2 = \Omega$ and always satisfies $g^{(2)}(0) \geqslant 1$, which means that the statistics of reflected photons cannot be sub-Poissonian and the photon blockade effect vanishes in the weak-coupling regime. The bunching behaviors exhibited by $g^{(2)}(\tau)$ of two reflected photons for $E/2 = \lambda_{1\pm}^{(0)}$ [solid (blue) curve in Fig. 4(c)] and Ω [solid (blue) curve in Fig. 4(d)] also illustrate the vanishing of the photon blockade effect. In addition, $g^{(2)}(\tau)$ of antibunched and bunched transmitted photons for $E/2 = \Omega$ and $\lambda_{1\pm}^{(0)}$ are shown by the dashed (red) curve in Figs. 4(c) and . 4(d).

IV. CONCLUSION

We have analytically studied the two-photon transport in a waveguide coupled to the cavity containing TLS, and explored the conditions for the photon blockade effect and single-photon generation in reflection. The two-photon statistical

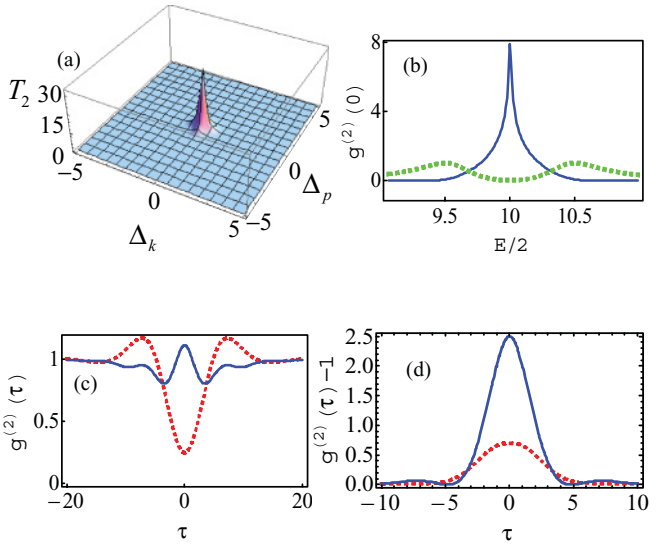

FIG. 4. (Color online) The two-photon background fluorescence and the correlation functions for the weak-coupling regime; the system parameters are the same as that in Fig. 2: (a)–(c) represent the same physical meaning in Fig. 2; (d) $[g^{(2)}(\tau) - 1]/10^{11}$ of the reflected [solid (blue) curve] photons for $E/2 = \Omega$ and $[g^{(2)}(\tau) - 1]/10^{10}$ of transmitted [dashed (red) curve] photons for $E/2 = \lambda_{1s}^{(0)}$.

characteristics of the outgoing photons obtained from an exactly analytic formula agree with the observations of a recent experiment [19]. Our theoretical approach can also be generalized to the scattering problems in systems with artificial atoms [50]. Using the LSZ approach developed in our paper, we can study the multiphoton processes and explore the mechanism [16,23] for the single-photon source. On the other hand, we can also generalize the LSZ approach to study the quantum state transfer of photons in the complex quantum network.

ACKNOWLEGMENT

This work is supported by National Natural Science Foundation of China under Grants No. 10935010 and No. 11074261.

APPENDIX: LSZ REDUCTION FOR PHOTON SCATTERING

In this Appendix, we briefly review how the LSZ reduction approach works in quantum optics. In quantum optics, we constantly consider how the optical systems, e.g., the linear or nonlinear cavity, affect the quantum properties of the incident photons. Usually, one can use the input-output theory, the quantum trajectory method, the master equation method, and so on. Here, we consider the problem by scattering method, i.e., solving the S matrix for the incident photons scattered by the optical systems and obtaining the scattering wave function. By the wave function of outgoing photons, we can investigate the quantum statistics of the output photons. Fortunately, the LSZ reduction approach relates to the Green function and S matrix for photons, and we can obtain an S matrix by solving the Green function of photons. For some special case, e.g., the linear dispersion of the scattering photons, the photonic

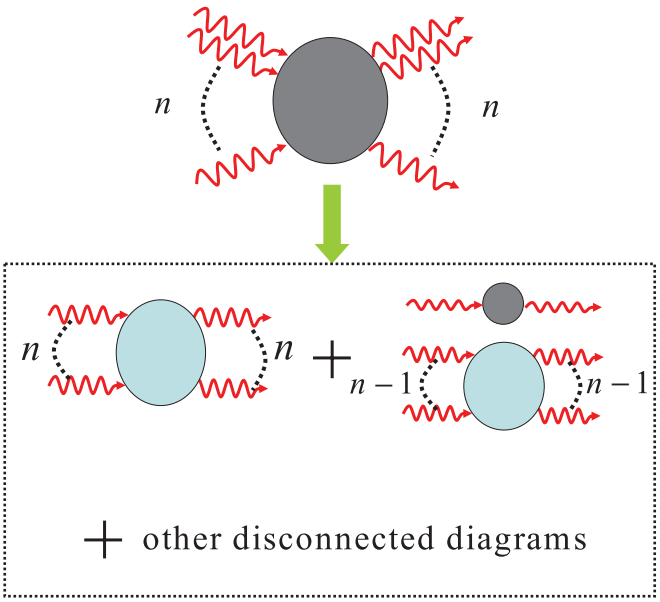

FIG. 5. (Color online) The Feynman diagrams for LSZ reduction: The red wavy line denotes the free photon propagator. The gray dark circles denote the S-matrix elements and the blue bright circles denote the T-matrix elements. The Feynman diagram of the S-matrix element is constructed by all kinds of disconnected diagrams, and each of the disconnected diagrams contains some connected diagrams.

Green function can be exactly calculated, so that the S matrix is analytically obtained.

First, we need to give their definitions for discussing the LSZ reduction explicitly. The $2n$-point Green's function

$$G_{p_1,\ldots,p_n;k_1,\ldots,k_n}(t'_1,\ldots,t'_n;t_1,\ldots,t_n) = \langle\Theta|T a_{p_1}(t'_1)\cdots a_{p_n}(t'_n)a^\dagger_{k_1}(t_1)\cdots a^\dagger_{k_n}(t_n)|\Theta\rangle \quad \text{(A1)}$$

is defined by the time-ordering product T of the photon creation (annihilation) operator $a^\dagger_k(a_k)$ in the Heisenberg picture. Here, Θ denotes the ground state of the Hamiltonian H of the system.

The S-matrix element

$${}_{\rm out}\langle f|i\rangle_{\rm in} = {}_{\rm in}\langle f|S|i\rangle_{\rm in} \quad \text{(A2)}$$

is defined through the overlap of incident state $|i\rangle_{\rm in}$ and outgoing scattering state $|f\rangle_{\rm out}$, where the incoming state is

$$|i\rangle_{\rm in} = a^\dagger_{k_1}\cdots a^\dagger_{k_n}|0\rangle. \quad \text{(A3)}$$

In the interaction picture, the S matrix is given by

$$S = T\ \exp\left(-i\int_{-\infty}^{+\infty} dt\ H_{\rm int}(t)\right). \quad \text{(A4)}$$

Here, $H_{\rm int}$ denotes the interaction between the photons and the optical systems.

It follows from the diagrammatic analysis that the Feynman diagram of the S-matrix element is contributed from all kinds of disconnected diagrams as shown in Fig. 5. Here, each of these disconnected diagrams contains some connected diagrams corresponding to the T-matrix elements.

For the single-photon case, the S-matrix element

$$S_{p;k} = \delta_{kp} + iT_{p;k} \quad \text{(A5)}$$

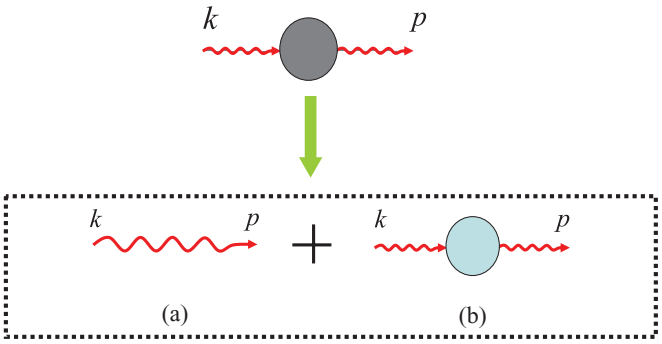

FIG. 6. (Color online) The diagrammatic constructions of the single-photon S-matrix element: There exist two kinds of disconnected diagrams, (a) and (b). The red wavy line denotes the free photon propagator. The gray dark circle denotes the S-matrix elements and the blue bright circle denotes the single-photon T-matrix elements.

is defined by the T-matrix element for the single photon, where k and p are the momenta of the incoming and outgoing photons. In this case, there exist two kinds of disconnected diagrams, (a) and (b), as shown in Fig. 6. For the two-photon case, the S-matrix element

$$S_{p_1p_2;k_1k_2} = S_{p_1k_1}S_{p_2k_2} + S_{p_2k_1}S_{p_1k_2} + iT_{p_1p_2;k_1,k_2} \quad \text{(A6)}$$

is reduced by the T-matrix element of two photons, where k_r and p_r $(r = 1,2)$ are the momenta of the incoming and outgoing photons. We have shown the two-photon reduction processes in the text. Obviously, the multiphoton S matrix is totally determined by the connected T matrix, so we only find the T matrices.

The intrinsic relation

$$iT_{2n} = G_{2n}\prod_{r=1}^{n}\left[2\pi\ G_0^{-1}(k_r)G_0^{-1}(p_r)\right]\Big|_{\rm os} \quad \text{(A7)}$$

between the n-photon T-matrix element

$$T_{2n} = T_{p_1,\ldots,p_n;k_1,\ldots,k_n} \quad \text{(A8)}$$

and Green's function

$$G_{2n} = G_{p_1,\ldots,p_n;k_1,\ldots,k_n} \quad \text{(A9)}$$

is given by the LSZ reduction formula, where

$$G_0(k_r) = \frac{i}{\omega_r - \varepsilon_{k_r} + i0^+} \quad \text{(A10)}$$

is the Green function of the free photon and $G_{p_1,\ldots,p_n;k_1,\ldots,k_n}$ is the Fourier transformation of Eq. (A1). Here, the subscript os denotes the on-shell limit $\omega \to \varepsilon_k$. Finally, the multiphoton S-matrix elements are determined by Green's functions entirely. For some special cases, e.g., the linear dispersion of the incident photons, the Green function can be obtained exactly due to the quadratic form of the action. By the exact many-photon Green function, we can obtain the T matrix and S matrix.

[1] D. F. Walls and G. J. Milburn, *Quantum Optics* (Springer-Verlag, Berlin-Heidelberg, 2008).

[2] H. J. Kimble, Nature (London) **453**, 1023 (2008).

[3] A. Blais, R. S. Huang, A. Wallraff, S. M. Girvin, and R. J. Schoelkopf, Phys. Rev. A **69**, 062320 (2004).

[4] F. Marquardt and S. M. Girvin, Physics **2**, 40 (2009).

[5] P. Zhang, Y. D. Wang, and C. P. Sun, Phys. Rev. Lett. **95**, 097204 (2005).

[6] F. Xue, L. Zhong, Y. Li, and C. P. Sun, Phys. Rev. B **75**, 033407 (2007).

[7] T. Aoki, B. Dayan, E. Wilcut, W. P. Bowen, A. S. Parkins, T. J. Kippenberg, K. J. Vahala, and H. J. Kimble, Nature (London) **443**, 671 (2006).

[8] T. Yoshie, A. Scherer, J. Hendrickson, G. Khitrova, H. M. Gibbs, G. Rupper, C. Ell, O. B. Shchekin, and D. G. Deppe, Nature (London) **432**, 200 (2004).

[9] A. Badolato, K. Hennessy, Mete Atatüre, J. Dreiser, E. Hu, P. M. Petroff, and A. Imamoğlu, Science **308**, 1158 (2005).

[10] D. Englund, A. Faraon, I. Fushman, N. Stoltz, P. Petroff, J. Vučković , Nature (London) **450**, 857 (2007).

[11] K. Hennessy, A. Badolato, M. Winger, D. Gerace, M. Atatüre, S. Gulde, S. Fält, E. L. Hu, and A. Imamoğlu, Nature (London) **445**, 896 (2007).

[12] I. Fushman, D. Englund, A. Faraon, N. Stoltz, P. Petroff, and J. Vučković, Science **320**, 769 (2008).

[13] A. Wallraff, D. I. Schuster, A. Blais, L. Frunzio, R. S. Huang, J. Majer, S. Kumar, S. M. Girvin, and R. J. Schoelkopf, Nature (London) **431**, 162 (2004).

[14] K. Srinivasan and O. Painter, Nature (London) **450**, 862 (2007).

[15] B. Dayan, A. S. Parkins, T. Aoki, E. P. Ostby, K. J. Vahala, and H. J. Kimble, Science **208**, 1062 (2008).

[16] A. Imamoğlu, H. Schmidt, G. Woods, and M. Deutsch, Phys. Rev. Lett. **79**, 1467 (1997).

[17] P. Grangier, D. F. Walls, and K. M. Gheri, Phys. Rev. Lett. **81**, 2833 (1998).

[18] K. M. Gheri, W. Alge, and P. Grangier, Phys. Rev. A **60**, R2673 (1999).

[19] K. M. Birnbaum, A. Boca, R. Miller, A. D. Boozer, T. E. Northup, and H. J. Kimble, Nature (London) **436**, 87 (2005).

[20] A. Kubanek, A. Ourjoumtsev, I. Schuster, M. Koch, P. W. H. Pinkse, K. Murr, and G. Rempe, Phys. Rev. Lett. **101**, 203602 (2008).

[21] A. Badolato, M. Winger, K. J. Hennessy, E. L. Hu, and A. Imamoğlu, C. R. Phys. **9**, 850 (2008).

[22] S. Rebic, S. M. Tan, A. S. Parkins, and D. F. Walls, J. Opt. B **1**, 490 (1999).

[23] M. J. Werner and A. Imamoğlu, Phys. Rev. A **61**, 011801 (1999).

[24] M. Bamba, A. Imamoğlu, I. Carusotto, and C. Ciuti, Phys. Rev. A **83**, 021802 (2011).

[25] P. Michler, A. Kiraz, C. Becher, W. V. Schoenfeld, P. M. Petroff, Lidong Zhang, E. Hu, and A. Imamoğlu, Science **290**, 2282 (2000).

[26] J. P. Reithmaier, G. Sek, A. Löffler, C. Hofmann, S. Kuhn, S. Reitzenstein, L. V. Keldysh, V. D. Kulakovskii, T. L. Reinecke, and A. Forchel, Nature (London) **432**, 197 (2004).

[27] T. Yoshie, A. Scherer, J. Hendrickson, G. Khitrova, H. M. Gibbs, G. Rupper, C. Ell, O. B. Shchekin, and D. G. Deppe, Nature (London) **432**, 200 (2004).

[28] E. Ginossar, L. S. Bishop, D. I. Schuster, and S. M. Girvin, Phys. Rev. A **82**, 022335 (2010).

[29] A. Faraon, A. Majumdar, and J. Vučković, Phys. Rev. A **81**, 033838 (2010).

[30] D. G. Angelakis, M. F. Santos, and S. Bose, Phys. Rev. A **76**, 031805 (2007).

[31] M. K. Olsen, J. J. Hope, and L. I. Plimak, Phys. Rev. A **64**, 013601 (2001).

[32] R. J. Brecha, P. R. Rice, and M. N. Xiao, Phys. Rev. A **59**, 2392 (1999).

[33] L. Tian and H. J. Carmichael, Phys. Rev. A **46**, 6801 (1992).

[34] E. Waks and J. Vučković, Phys. Rev. Lett. **96**, 153601 (2006).

[35] R. J. Thompson, G. Rempe, and H. J. Kimble, Phys. Rev. Lett. **68**, 1132 (1992).

[36] K. Srinivasan and O. Painter, Phys. Rev. A **75**, 023814 (2007).

[37] H. Lehmann, K. Symanzik, and W. Zimmerman, Nuovo Cimento **1**, 205 (1955).

[38] T. Shi and C. P. Sun, Phys. Rev. B **79**, 205111 (2009); e-print arXiv:0907.2776.

[39] J. T. Shen and S. Fan, Phys. Rev. A **79**, 023837 (2009).

[40] E. Rephaeli, J. T. Shen, and S. Fan, Phys. Rev. A **82**, 033804 (2010).

[41] J. T. Shen and S. Fan, Phys. Rev. Lett. **95**, 213001 (2005); **98**, 153003 (2007); Opt. Lett. **30**, 2001 (2005).

[42] L. Zhou, Z. R. Gong, Y. X. Liu, C. P. Sun, and F. Nori, Phys. Rev. Lett. **101**, 100501 (2008).

[43] L. Zhou, J. Lu, and C. P. Sun, Phys. Rev. A **76**, 012313 (2007).

[44] H. Dong, Z. R. Gong, H. Ian, Lan Zhou, and C. P. Sun, Phys. Rev. A **79**, 063847 (2009).

[45] M. Hillery and M. S. Zubairy, Phys. Rev. A **26**, 451 (1982).

[46] M. Hillery and M. S. Zubairy, Phys. Rev. A **29**, 1275 (1984).

[47] C. P. Sun, Phys. Scr. **48**, 393 (1993).

[48] J. T. Shen and S. Fan, Phys. Rev. Lett. **98**, 153003 (2007); **76**, 062709 (2007).

[49] M. Fabrizio and A. O. Gogolin, Phys. Rev. B **51**, 17827 (1995).

[50] O. Astafiev, A. M. Zagoskin, A. A. Abdumalikov Jr., Yu. A. Pashkin, T. Yamamoto, K. Inomata, Y. Nakamura, and J. S. Tsai, Science **327**, 840 (2010).